Low energy effective area of the *Chandra* low energy transmission grating spectrometer

D. Pease, J.J. Drake, C.O. Johnson, V. Kashyap, R.P. Kraft, P.W. Ratzlaff, B.J. Wargelin
Harvard-Smithsonian Center for Astrophysics, Cambridge, MA 02138

A.C. Brinkman, J.S. Kaastra, R.L.J. van der Meer, F.B. Paerels
Space Research Organisation Netherlands (Netherlands)

V. Burwitz, P. Predehl
Max-Planck-Institut für Extraterrestrische Physik (Germany)

H.L. Marshall
Center for Space Research, M.I.T., Cambridge, MA

M.A. Barstow
University of Leicester, Leicester LE1 7RH (UK)

D.S. Finley
Eureka Scientific, Oakland, CA

J. Dupuis
Space Sciences Laboratory, University of California, Berkeley, CA

ABSTRACT

The *Chandra X-ray Observatory* was successfully launched on July 23, 1999, and subsequently began an intensive calibration phase. We present preliminary results from in-flight calibration of the low energy response of the High Resolution Camera Spectroscopic readout (HRC-S) combined with the Low Energy Transmission Grating (LETG) aboard *Chandra*. These instruments comprise the Low Energy Transmission Grating Spectrometer (LETGS). For this calibration study, we employ a pure hydrogen non-LTE white dwarf emission model ($T_{\rm eff}$ = 25000 K and $\log g = 9.0$) for comparison with the *Chandra* observations of Sirius B. Pre-flight calibration of the LETGS effective area was conducted only at wavelengths shortward of 45 Å (E > 0.277 keV). Our Sirius B analysis shows that the HRC-S quantum efficiency (QE) model assumed for longer wavelengths overestimates the effective area on average by a factor of 1.6. We derive a correction to the low energy HRC-S QE model to match the predicted and observed Sirius B spectra over the wavelength range of 45-185 Å. We make an independent test of our results by comparing a *Chandra* LETGS observation of HZ 43 with pure hydrogen model atmosphere predictions and find good agreement.

Keywords: *Chandra*, X-ray, X-ray spectroscopy, transmission grating, calibration

1. INTRODUCTION

The in-flight science instrument calibration of the *Chandra X-ray Observatory* began in August 1999. The goal of the LETGS calibration effort is to calibrate the response of the LETGS over its entire active energy range of 0.065−6.0 keV (wavelengths 2−200 Å). Prior to in-flight calibration, the HRC-S QE was calibrated over the energy range of 0.277−10.0 keV. QE calibration below 0.277 keV was incomplete, and an estimate was provided for observation planning. The first phase of calibration observations has provided us with the first tests of the performance of the LETGS over the low energy range.

Send correspondence to DP; E-mail: pease@head.cfa.harvard.edu
Copyright 2000 Society of Photo-Optical Instrumentation Engineers.
This paper was published in *X-Ray Optics, Instruments, and Missions III*, Joachim E. Trümper, Bernd Aschenbach, Editors, Proceedings of SPIE Vol. 4012, p. 700, and is made available as an electronic reprint with permission of SPIE. One print or electronic copy may be made for personal use only. Systematic or multiple reproduction, distribution to multiple locations via electronic or other means, duplication of any material in this paper for a fee or for commercial purposes, or modification of the content of the paper are prohibited.

The low energy calibration of the LETGS is best achieved by observing nearby hot white dwarfs. White dwarfs with effective temperatures greater than 20000 K and photospheres composed of pure hydrogen should produce featureless continua that can be used to derive any real variations in the response. Furthermore, the photospheric models of hot white dwarfs are considered to be well understood, and their X-ray emission covers the low energy range of interest (0.065−0.277 keV, $\lambda > 45$ Å). The geometry of the HRC-S/LETG dispersion simplifies calibration by constraining all observable emission to 1st order.

The white dwarfs chosen as calibration targets are Sirius B and HZ 43. Sirius B is our primary target for the low energy calibration effort. It is the nearest white dwarf, the secondary of the binary system α CMa. Recent analyses of Sirius B observations by EXOSAT, EUVE, and IUE have led to precision in the determination of its fundamental parameters $T_{\rm eff}$ and $\log g$ (Holberg *et al.* 1998). As a result, we are most confident of the emission models for Sirius B and have adopted the model parameters $T_{\rm eff} = 25000$ K and $\log g = 9.0$ (Holberg *et al.* 1998).

HZ 43 is brighter in X-rays than Sirius B; however, we have less confidence in the knowledge of model parameters. We therefore use it as a comparison check with our Sirius B analysis. Additionally, since HZ 43 is relatively bright, it will be useful for monitoring the QE with minimal observation time required. For HZ 43 we adopt $T_{\rm eff} = 51000$ K and $\log g = 7.9$ (Barstow *et al.* 1997).

For energies in the mid-range of the LETGS (0.2−0.8 keV, $\lambda < 60$ Å) we observed the bright and relatively nearby quasar 3C 273 ($z = 0.158$). By applying a simple power-law emission model, we perform an analysis procedure similar to that with the white dwarfs and attempt to derive corrections for the LETGS effective area over this energy range. 3C 273 is a much harder source than the white dwarfs, with X-ray emission up to the LETGS high energy limit of ~ 6.0 keV. The hard spectrum (E > 1.0 keV) has been well-fit with a power-law index of $\Gamma \cong 1.6$ (Kriss *et al.* 1999; Orr *et al.* 1998; Yaqoob, Serlemitsos, Mushotzky 1994). The analysis of 3C 273, however, has several complications. The spectrum shows a possible break over 0.5−1.0 keV, which can be modeled by a compound power-law (Kriss *et al.* 1999; Leach, McHardy, Papadakis 1995). The energy range of the break overlaps our range of interest. Analysis is further complicated by LETGS high order contributions. For this preliminary work we adopt a single power-law model with $\Gamma = 1.62$ which provides a reasonable fit to the data when a significant amount of high order contribution is considered.

In § 2. we present the observations and discuss background subtraction and spectral extraction; in § 3. we derive a correction to the effective area, from which we derive a new HRC-S QE and rebuild the LETGS effective area for the low energy range intrinsically correlated with the LETGS dispersion; and in § 4. we discuss further work towards a complete calibration of the LETGS over its entire active energy range.

2. OBSERVATIONS AND DATA REDUCTIONS

2.1. HRC-S Background Reduction: Pulse-Height Amplitude Filtering

The background rate in the HRC-S is much higher than pre-flight expectations due to a timing error in its anti-coincidence shield. Currently, the HRC-S rate is about 7×10^{-5} counts s^{-1} arcsec^{-2}, or 0.12 counts per pixel in 10^5 seconds. A dispersed line in the LETGS is between about 20 and 65 pixels tall (cross-dispersion direction) and 7 pixels wide (FWHM), and therefore lies on top of roughly 15−55 background counts in a 10^5 second exposure.

Fortunately, the HRC-S background can be reduced by factors of a few to several by appropriate data filtering. Included in the *Chandra* image files are data recording various signal amplitudes associated with each detected event. The most important of these signals is the "pha" (pulse height amplitude), which records the total collected charge for each event. Excluding the highest pha channel (255) reduces the background by typically 25% with a negligible ($\ll 1\%$) loss of X-ray events. Larger reductions (up to $\sim 80\%$) can be attained by using position-dependent pha filtering. This is made possible by: the small but useful energy resolution of the HRC-S; the difference in pha distributions of X-ray and particle background events; and the known correspondence of photon energy with detector position for grating-dispersed spectra. For monochromatic photons incident upon the HRC-S, the 1σ width of the pha distribution *at a given point on the detector* is about 0.22 times the mean pha value. The distribution for background events, in contrast, is relatively broad and flat (see Figure 1). By selecting a range of pha values around the X-ray mean, one can then exclude events outside the specified pha range, greatly reducing the number of background events with little loss of X-ray events. To implement the filtering with ease, we have developed a pha-filtering software tool. Further details of our HRC-S background filtering process will be published elsewhere by Wargelin *et al.*

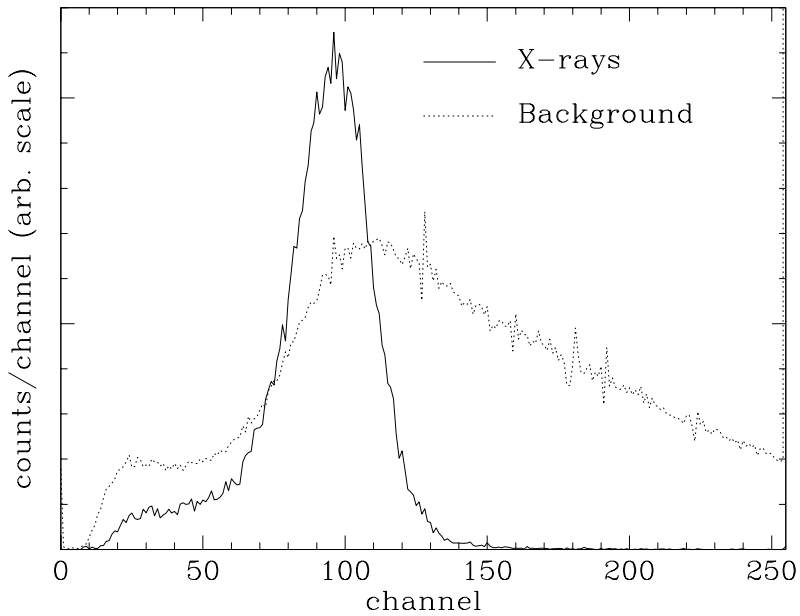

Figure 1. Pulse height spectra of X-rays and background. X-ray spectrum is a sum taken from detector regions (128 × 128 pixels in size) where the mean pha value = 90±1. The contribution from background, which is less than 4%, has been subtracted. Background spectrum is taken from a larger area. Channel 255, which contains roughly 25% of the background events, has been truncated for display purposes.

Preliminary tests of our pha-filtering tool show typical background reductions of 60% with 2% X-ray loss, 65% with 5% X-ray loss, and 75% with 15% X-ray loss. Results using a background spectrum from an observation of the binary star, Capella, are shown in Figure 2. Note that filtering is more effective at long wavelengths, where the peak of the X-ray pha distribution is further below the mean of the background pha distribution. It is expected that minimal ($\leq$ 2% X-ray loss) pha-filtering will become a part of the standard data processing pipeline by April 2000. Observers can then apply tighter filtering as their particular needs require.

2.2. Low Energy Calibration Observations and Spectral Extractions

The observations from which we calibrate the low energy response of the LETGS are listed in Table 1. Three observations of Sirius B (*Chandra* OBSIDs 1421,1452,1459), with a total valid observation time of 41178 seconds, were co-added to maximize signal-to-noise. HZ 43 (OBSID 59) and 3C 273 (OBSID 460) were each observed only once, for 39833 seconds and 40300 seconds, respectively. The absorption column densities relevant to these observations are compiled in Table 2.

Table 1. LETGS Calibration Observations

OBSID(s)	Target	Exposure Time (ksec)
(1421,1452,1459) co-added	Sirius B	40.2
59	HZ 43	39.9
460	3C 273	40.3

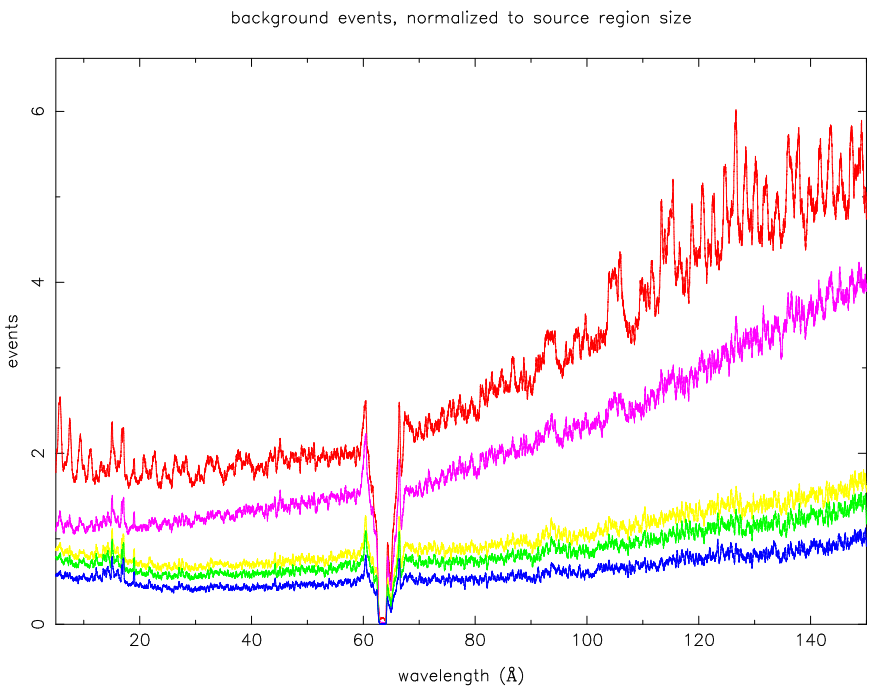

Figure 2. The LETG+HRC-S background spectrum for an observation of Capella using an optimized parabolic spectral extraction window and filtered by pulse height to different levels of X-ray loss (see text). The curves from the top down correspond to: no filtering; pha=255 events removed with 0% X-ray event loss; filtering with 2% X-ray loss; 5% X-ray loss; and 15% X-ray loss. The units of the y axis are total events/bin with a bin size of one pixel (6.43 μm, or .0074 Å). Exposure time was 85 ksec.

Table 2. H I, He I, He II column densities

Target	log $N_{\rm H\ I}$ ($\rm cm^{-2}$)	log $N_{\rm He\ I}$ ($\rm cm^{-2}$)	log $N_{\rm He\ II}$ ($\rm cm^{-2}$)	Reference
Sirius B	17.72	16.77	16.34	Holberg *et al.* 1998
HZ 43	17.94	16.81	16.64	Barstow *et al.* 1997
3C 273	20.26	19.22	18.26	Stark *et al.* 1992

The spectra were extracted using a procedure we have developed to optimize signal-to-noise for the LETGS dispersion. For the HRC-S QE analysis we wanted to retain as much data as possible, so the observations were filtered conservatively for background (pha=5−200 for $\leq$ 2% source X-ray loss; as described in § 2.1). The LETGS extraction region which we employ (Figure 3) is defined by two parabolae. Its width varies with wavelength and has been optimized to match the astigmatic cross-dispersion of the Rowland circle geometry, while including as much of the diffracted spectrum as possible and minimizing the included background. The background regions are taken just outside the extraction region. The extraction efficiency varies from $\approx$ 90% for short wavelengths to $\approx$ 95% for longest wavelengths.

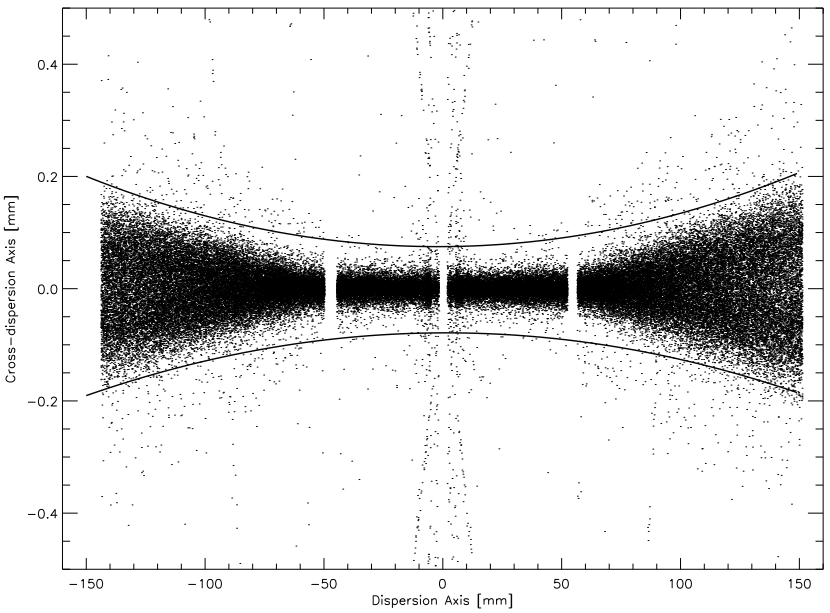

Figure 3. A simulation of a flat spectrum designed to illustrate the broadening of the LETGS profile in the cross-dispersion direction, and the effectiveness of the optimized parabolic spectral extraction region.

3. EFFECTIVE AREA AND QUANTUM EFFICIENCY ANALYSIS

The model of Sirius B for which we have the most confidence is a pure hydrogen non-LTE white dwarf emission model with $T_{\rm eff} = 25000$ K and $\log g = 9.0$ (Holberg *et al.* 1998). The flux uncertainties in this model are estimated to be less than 10%. Employing the model we derive a correction to the *Chandra* LETGS effective area for energies below C-Kα at 0.277 keV ($\lambda > 45$ Å). Though we make the initial correction in terms of the effective area, the fundamental correction is applied to the model of the HRC-S QE. The other components of the effective area (the High Resolution Mirror Assembly effective area, HRC-S UV/ion shield transmission, LETG efficiency, and the extraction region efficiency) are independently calibrated with good accuracy. The corrections we present here are intrinsically linked to the dispersion of the LETG, as specific wavelengths/energies correspond to specific locations on the HRC-S. LETGS positive and negative spectral orders are treated separately.

In Figure 4, we show the pre-flight effective area model-predicted spectrum for Sirius B compared with the LETGS observed spectrum. The comparison suggests that the pre-flight HRC-S QE overestimates the spectrum by an average factor of about 1.6.

We correct the effective area by taking the ratio of the pre-flight model and the in-flight data. We smooth the curves by binning the data by 100 pixels (1 pixel = 0.0074 Å). The derived correction curves are shown in Figure 5. We assume that the pre-flight model is good for energies greater than 0.277 keV, and we force the ratio to be 1.0 at this energy and above. The energy 0.277 keV also corresponds to the limit of usefulness of Sirius B; the white dwarf has no measurable emission shortward of 45 Å (E > 0.277 keV).

Applying the correction curves to the HRC-S QE model, we rebuild the LETGS effective area. The resultant "corrected" LETGS effective area is shown in Figure 6. Figure 7 shows the "corrected model" spectrum overlayed on the Sirius B data. Indeed, our model now has "perfect" agreement with the data below 0.277 keV. In Figure 8 two model-predicted spectra of HZ 43 ($T_{\rm eff} = 51000$ K and $\log g = 7.9$, Barstow *et al.* 1997; and D.S. Finley) generated with the new HRC-S QE are compared to the LETGS observed spectrum. The independent agreements between these models and the data are good to 10−15%, which is within the uncertainties in the models.

For the calibration of the mid-range energies linking the new low energy response to the previously calibrated response above 0.277 keV, we use the quasar 3C 273. We derive our power-law parameters ($\Gamma = 1.62$ and norm $= 0.025$) from a preliminary fit of an ACIS+HETG spectrum of 3C 273. This *Chandra* instrument combination is optimized for the higher energy targets, and unlike the HRC-S, it is capable of separating spectral orders.

There are some complications inherent in using 3C 273 for this calibration. For example, there are a wide variety of power-law photon indices reported in the literature for different energy bands of the 3C 273 spectrum. Also, there are differing opinions over where (and whether or not) a simple power-law breaks into a compound power-law. As a result, there are many ways to achieve a reasonable fit of the power-law model to the data. One way is to vary the index Γ. Another is to employ a 2-part power-law model with a break in the 0.5−1.0 keV energy range.

For proper analysis of LETGS spectrum of 3C 273 it is essential to include higher order flux. The importance of higher orders is illustrated in Figure 9. The dashed curve shows the single power-law model computed for 1st order only, compared with the LETGS observed spectrum. This model falls 20−50% below the observed data over the energy range of 0.2−0.8 keV ($\lambda \approx 15-60$ Å). However, we find a good fit with $\Gamma = 1.62$, if a significant contribution to the spectrum by higher orders is considered. The solid curve in Figure 9 shows the model with LETGS orders 1−5 summed (Σ O(1−5)) compared with the observed spectrum. From this analysis it looks quite reasonable to employ a simple, single power-law model. The "fit" suggests that our current model of the HRC-S QE above 0.277 keV is good. Though the uncertainties in model parameters and order contributions make the process of absolute calibration with 3C 273 complicated, broadband QE verification with 3C 273 indicates that our current model of HRC-S QE over the energy range 0.2−0.8 keV ($\lambda \approx 15-60$ Å) is good to $\sim 15\%$.

In Figure 10 we show the in-flight calibrated *Chandra* LETGS effective area for 0th order on-axis, combined positive and negative dispersed 1st order, 2nd order and 3rd order.

4. CONCLUSIONS AND FUTURE DIRECTIONS

As a result of the recent in-flight calibration effort, we have a much better understanding of the LETGS low energy response. Preliminary study has revealed that the pre-flight HRC-S QE model overestimates the true response by an average factor of about 1.6. With this new knowledge, we have calibrated the *Chandra* LETGS below 0.277 keV, and have derived an HRC-S QE intrinsically linked to the LETG dispersion, over the long wavelength range of 45−185 Å (E ≈ 0.065−0.277 keV). We will continue to monitor the low energy response for changes and will apply fine-tuning to the model as the need arises. There remains much work to be done over the mid-range of the LETGS, particularly in the region of 0.3−1.0 keV, as 3C 273 is a complicated source to model over these energies. It will most likely require a two-part broken power-law in order to get a more accurate calibration. A rigorous error analysis is also needed. Most of the errors presented here are simply the statistical errors associated with the data; there are many systematic errors which have not been treated properly. All of these issues are currently being addressed and LETGS calibration is on-going. Readers are referred to the LETGS Observer Information web page (`http://asc.harvard.edu/cal/Links/Letg/User/`) for more detailed and current information.

Special thanks to the many teams who have helped make *Chandra* a success. DP, JJD, COJ, VK, HLM, PWR, and BJW were supported by *Chandra X-ray Center* NASA contract NAS8-39073 during the course of this research.

REFERENCES

Barstow, M.A., Doobie, P.D., Holberg, J.B., Hubeny, I., Lanz, T., 1997, MNRAS, 286, 58

Grandi, P., *et al.* , 1997, A&A, 325, L17

Holberg, J.B., Barstow, M.A., Bruhweiler, F.C., Cruise, A.M., Penny,A.J., 1998, ApJ, 497, 935

Kriss, G.A., Davidsen, A.F., Zheng, W., Lee, G., 1999, ApJ, 527, 683

Leach, C.M., McHardy, I.M., Papadakis, I.E., 1995, MNRAS, 272, 221

Orr, A., Yaqoob, T., Piro, L., White, N.E., Grandi, P., 1998, A&A, 337, 685

Stark, A.A., Gamie, C.F., Wilson, R.W., Bally, J. Linke, R.A., Heiles, C., Hurwitz, M., 1992, ApJS, 79, 77

Wargelin, B.J., *et al.* , in preparation

Yaqoob, T., Serlemitsos, P., Mushotzky, R., 1994, PASP, 46, L49

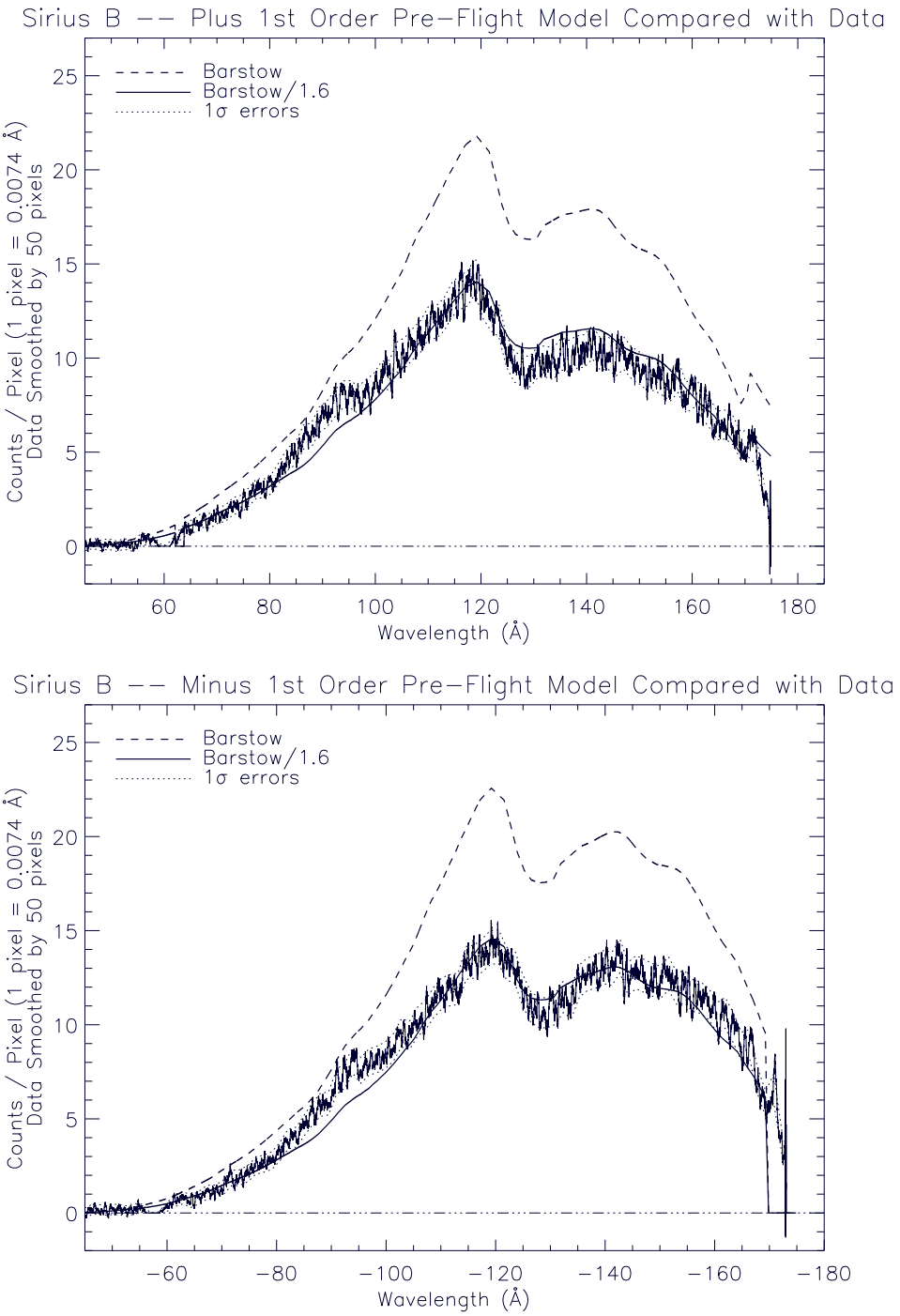

Figure 4. Comparison of the pre-flight model-predicted spectrum for Sirius B with the LETGS observed spectrum indicate that the pre-flight low energy HRC-S QE is overestimated by an average factor of about 1.6. Dashed line is the model, solid line is the model/1.6, and dotted lines are the 1σ statistical errors on the data. Positive and negative orders plotted separately.

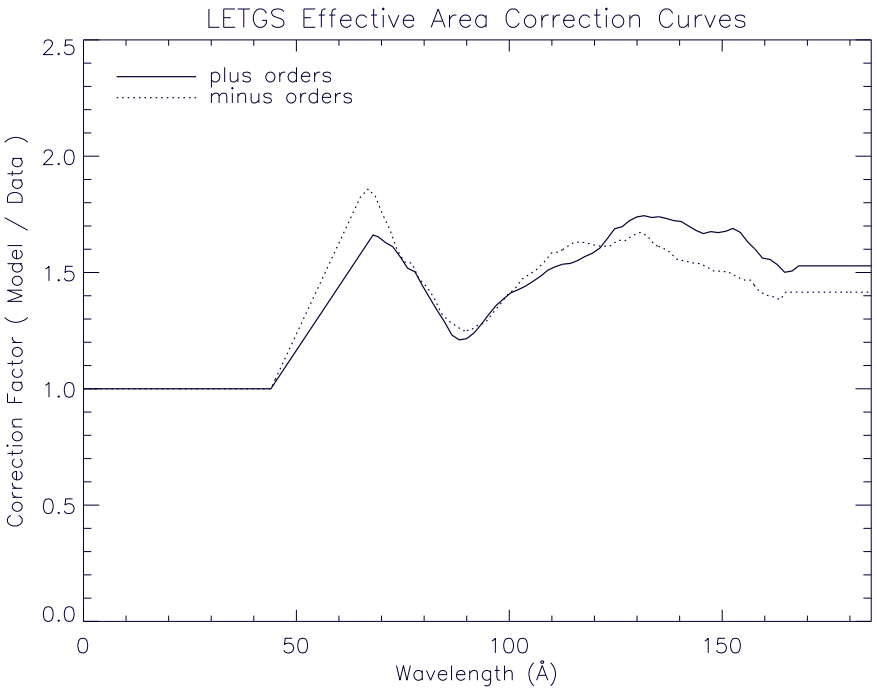

Figure 5. *Chandra* LETGS effective area correction curves derived from model-to-data comparison with Sirius B. Solid line is the correction to the positive orders and the dotted line is the correction to the negative orders.

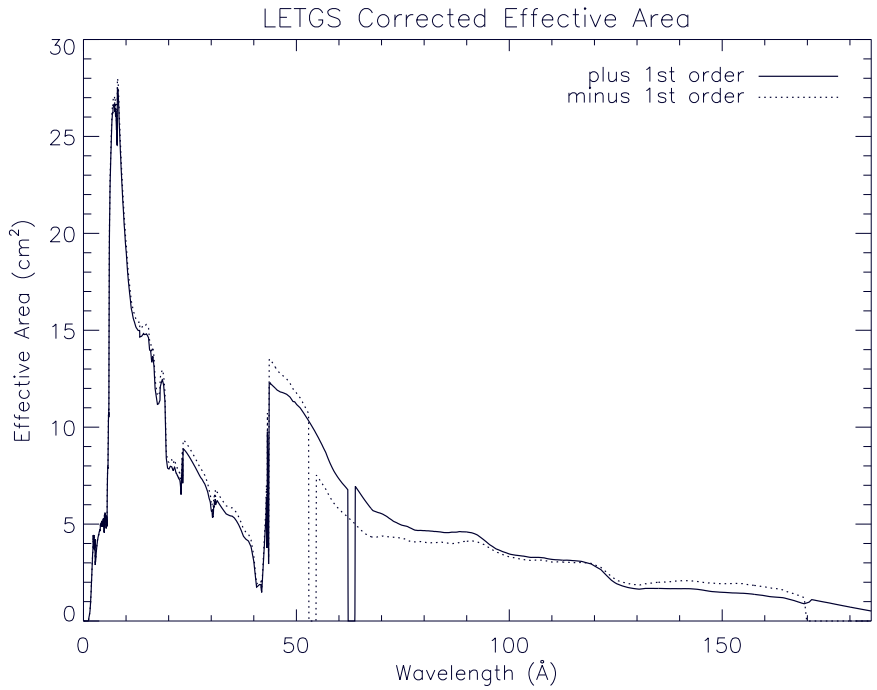

Figure 6. *Chandra* LETGS effective area, corrected at low energies (E $<$ 0.277 keV). The solid line is the positive 1st order and the dotted line is the negative 1st order. Dropouts to zero are caused by the plate gaps. Positive and negative order gaps occur at different wavelengths due to displacement of HRC-S center from telescope center.

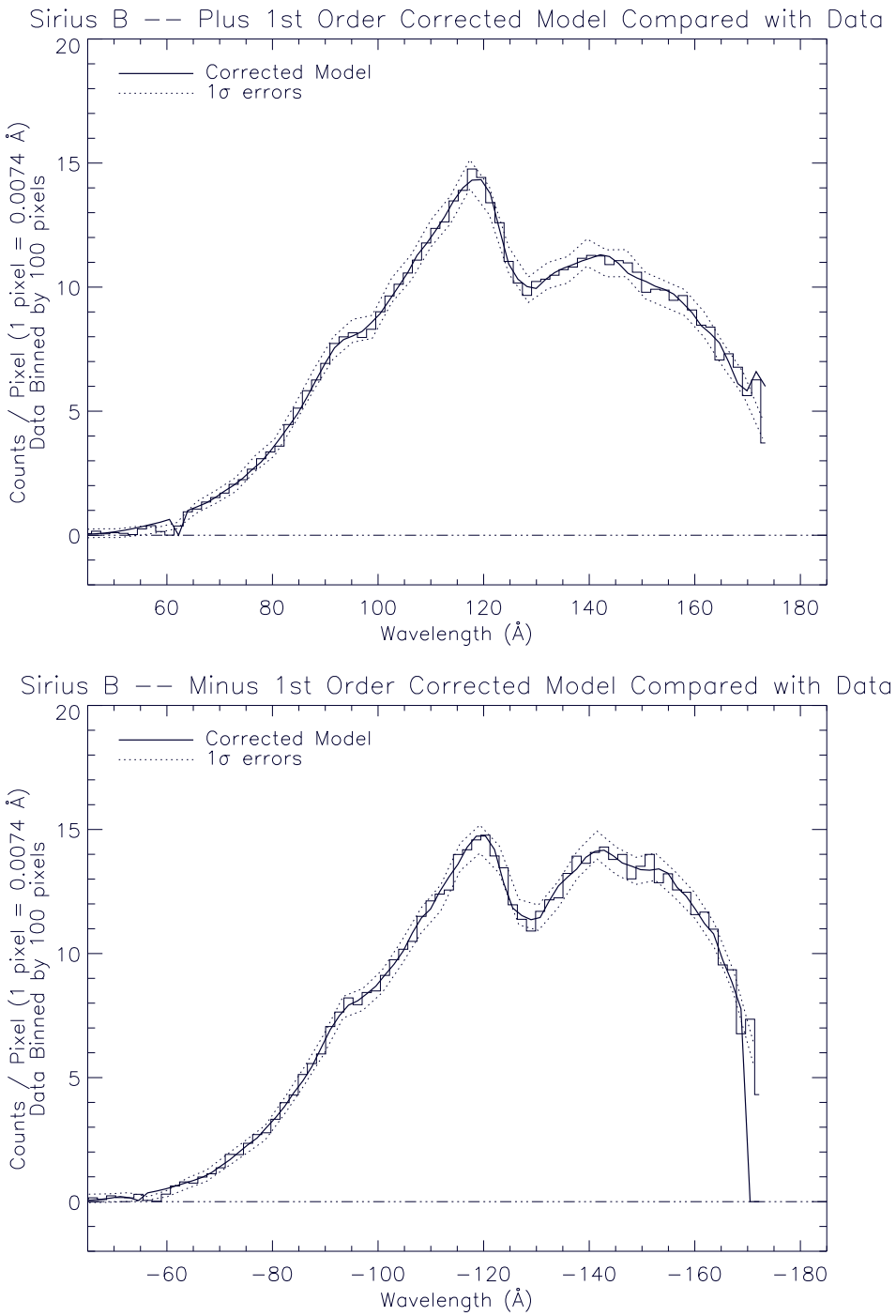

Figure 7. Re-Comparison of the "corrected" model-predicted spectrum for Sirius B with the LETGS observed spectrum. Positive and negative orders plotted separately.

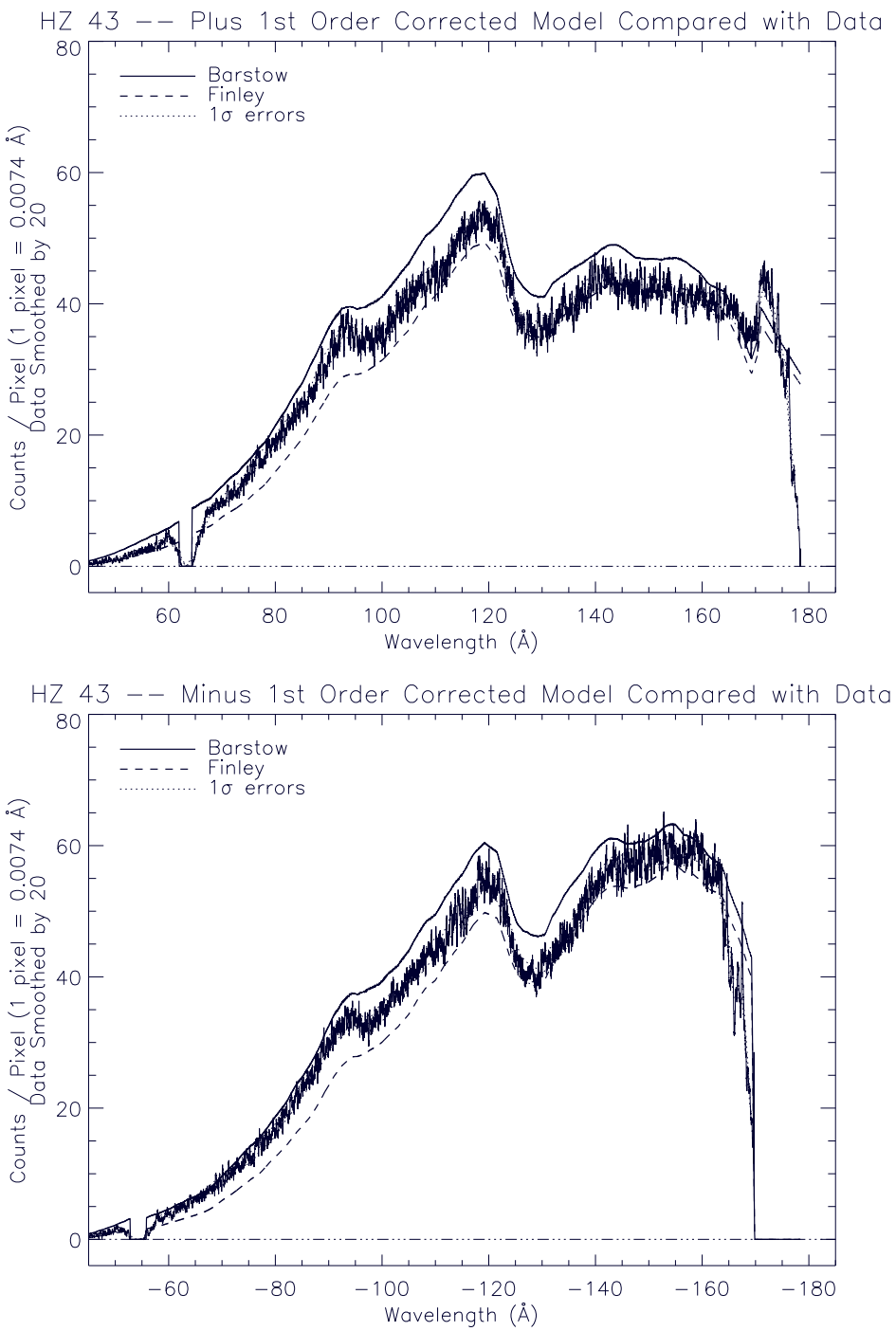

Figure 8. Comparison of two different model-predicted spectra for HZ 43 with the LETGS observed spectrum. Both models show good overall agreement with the data to $\approx 10\%$. Positive and negative orders plotted separately.

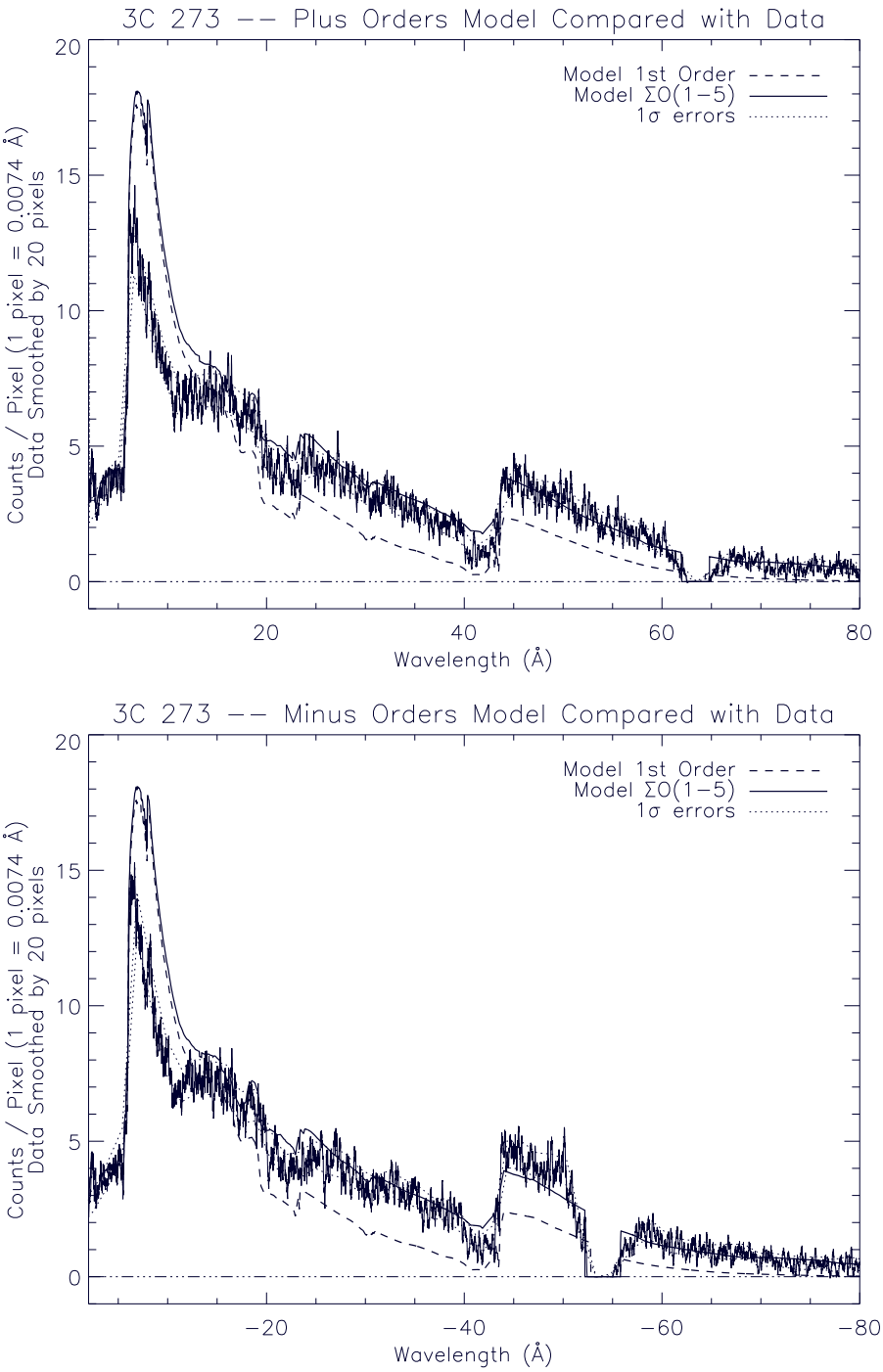

Figure 9. Comparison of the 1st order model-predicted spectrum (dashed curve) and the ΣO(1−5) model-predicted spectrum (solid curve) for 3C 273 with the LETGS observed spectrum. The summed orders model shows good agreement with the observed spectrum over the energy range 0.2−0.8 keV, illustrating the significance of high order contributions. Positive and negative orders plotted separately.

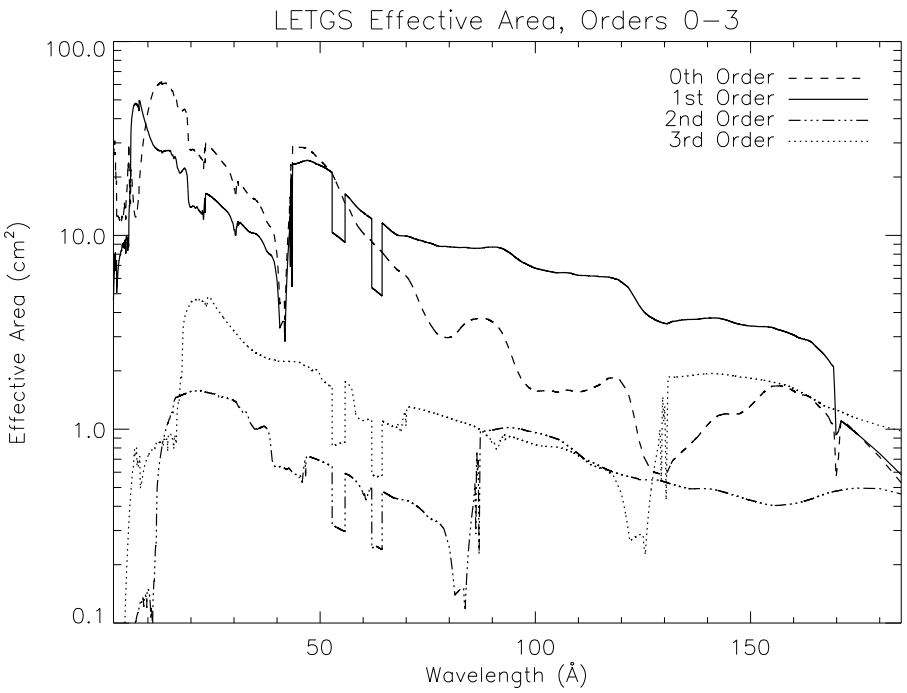

Figure 10. *Chandra* LETGS effective area for 0th order on-axis (dashed curve), 1st order dispersed (solid curve), 2nd order (dash-dot-dot-dot curve), and 3rd order (dotted curve). Dropouts are caused by the plate gaps. They do not go to zero because the positive and negative order gaps occur at different wavelengths due to the displacement HRC-S center from telescope center.